Nanometer-Scale Mapping of Defect-Induced Luminescence Centers in Cadmium Sulfide Nanowires

Ovidiu Cretu,[1,a)] Chao Zhang,[1,2] and Dmitri Golberg[1,2]

[1] *International Center for Materials Nanoarchitectonics (MANA), National Institute for Materials Science (NIMS), 1-1 Namiki, Tsukuba, Ibaraki 305-0044, Japan*

[2] *Graduate School of Pure and Applied Sciences, University of Tsukuba, 1-1-1 Tennodai, Tsukuba, Ibaraki 305-8577, Japan*

The luminescence centers in cadmium sulfide (CdS) nanowires are mapped through cathodoluminescence experiments inside a high resolution transmission electron microscope. This is made possible by positioning an optical fiber within a few micrometers of the area of interest and scanning the focused electron beam while simultaneously collecting the generated photons. The results reveal the distribution of luminescence centers in this material with nanometer-precision. Furthermore, these centers are associated to various intrinsic defects in CdS, which allows mapping these defects even when their concentration is far below the level detectable by other traditional techniques.

[a)] Author to whom correspondence should be addressed. Electronic mail: cretu.ovidiu@nims.go.jp.

Transmission electron microscopes (TEMs) are powerful instruments which make possible the structural and chemical characterization of materials down to the atomic scale.[1] There have been numerous attempts to extend the functionality of these apparatuses in order to allow interacting with the specimen while it is being imaged by the electrons; this has created the field of in situ TEM.[2,3] Cathodoluminescence (CL) is one of the in situ techniques that has emerged, taking advantage of the fact that the excitation of band-gap materials by the electron beam produces optical signals.[4] This technique has traditionally required large changes to the TEM column in order to insert mirrors[5] or optical fibers[6] which collect the generated photons, and has thus been reserved for dedicated instruments.

One-dimensional semiconducting nanostructures have been envisaged to be promising building blocks for next-generation electronic and optoelectronic devices. Some of their many potential applications include flexible displays and sensors, lithium-ion batteries, supercapacitors and solar cells.[7] Among the possible solids, CdS has attracted attention as a precursor material for these nanostructures due to its availability and ease of processing.[8] Some of its more attractive properties include direct bandgap, low work function, high refraction index and good chemical and thermal stabilities. As a result, this material has traditionally found applications in electronics, light emitting devices, and sensors.

In this work, we use in situ CL in order to characterize CdS nanowires (NWs) at the nanometer level, allowing us to obtain information which is not traditionally available at these length scales and to compare it with structural data produced by the high resolution TEM. We take a novel approach, which utilizes a specially-designed sample holder and requires no changes to the microscope itself. This creates significant advantages in terms of ease of implementation and portability. Our results permit us to map the contributions of various emission centers along the surface of the NW and to correlate these with the structural defects which produce them.

The CdS NWs used in this study were synthesized via a chemical vapor deposition (CVD) method, as described earlier.[9] The in situ experiments, as well as all of the imaging and electron diffraction, were performed using an energy-filtering Jeol JEM 3100FEF (Omega filter) high-resolution TEM operated at 300 kV. Micro-PL experiments on individual NWs were performed using a Horiba LabRam HR system equipped with a 325 nm HeCd excitation laser and a 200-1000 nm spectrometer. NIR PL experiments were carried out on the NW powder using a 532 nm excitation laser and a 900-1700 nm InGaAs detector. All measurements were performed at room temperature. The acquired data was processed using ImageJ[10] and Gatan Digital Micrograph.

The schematic layout of the system is illustrated in Figure 1. A multi-mode optical fiber with a 200 μm diameter core and a numerical aperture (NA) of 0.22 is mechanically connected to a piezoelectric tube, which allows for its positioning close to the region of interest of the sample with sub-nanometer accuracy, using a piezo-controller unit. The collection efficiency, determined by the acceptance cone of the fiber, is $\Omega = 2\pi(1-\cos\alpha) = 0.15$ srad, since $\sin\alpha = 0.22$. The sample is loaded onto an Au tip either via electrostatic interaction or by using a very small amount of conductive epoxy. The specimen holder is a modified version of a piezo-driven optical TEM holder (Nanofactory Instruments AB). A voltage source is connected to the scanning coils of the microscope and precisely controls the focused electron beam, which is scanned across the region of interest. The electrons interact with the sample and produce several signals: photons are collected by the optical fiber and transferred to a spectrometer, which uses a detector that operates in the visible range (300-1000 nm). The scattered electrons are collected by an annular electron detector and form an incoherent signal which is proportional to the mass-thickness of the specimen.[1] Both these signals are acquired simultaneously and mapped across the region of interest.

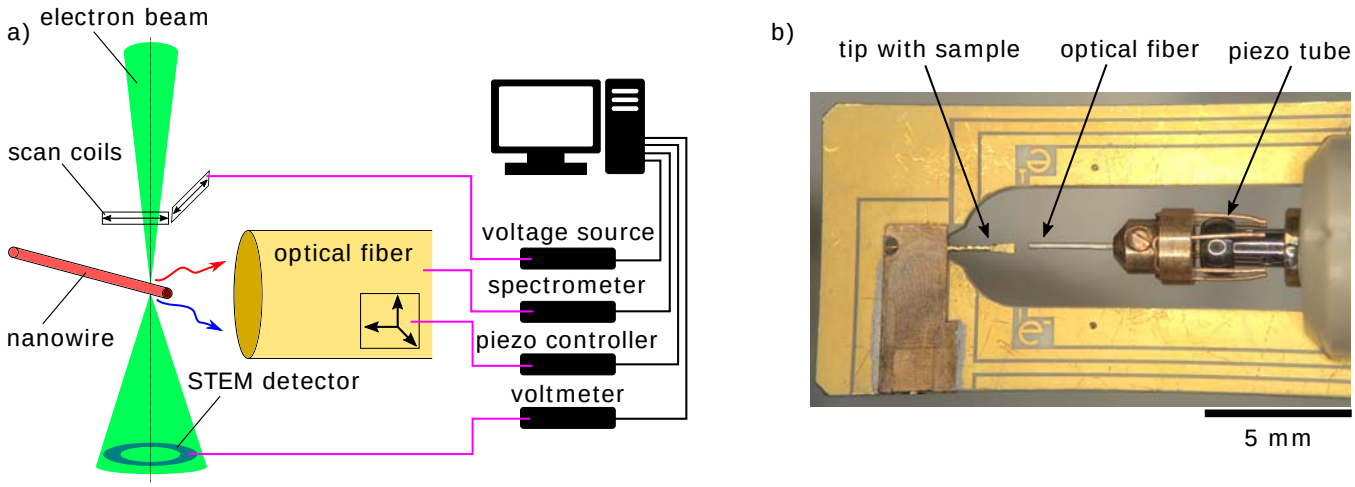

Figure 1. a) Schematic layout of the experimental set-up, showing the main components and interconnects. b) Optical image of the end-section of the holder, highlighting the locations of the sample, optical fiber and piezoelectric tube.

A low-magnification image of a NW is shown in Figure S1a in the supplementary material. It has a diameter of around 100 nm and a length of several micrometers, which is typical of the NWs that were tested. Figure S1b depicts a high-resolution image from the same NW, displaying good crystallinity. This is confirmed by the selected-area diffraction pattern in Figure S1c, which shows that these structures are indeed single crystals. While CdS can have different crystal structures,

we have found that the NWs correspond to the more stable wurtzite arrangement. This is highlighted in the diffraction pattern by spots corresponding to the (010), (011) and (002) lattice spacings.

The result of one of the experiments is summarized in Figure 2. Figure 2a shows the simultaneously-acquired dark-field image of the 200 nm-wide NW. In this particular case, the data is acquired from the last 1 μm-long section of the wire, which ends in the lower part of the image. Figure 2b and Figure 2c depict spectra acquired from two different regions in this section. An immediate observation is that the two spectra are quite different. One of our most important findings is that, for all the structures which we have examined, there is significant variability between signals coming from areas found in close proximity to each other.

We have investigated the possibility that these signals are caused by a superposition of the same component signals, with changing amplitudes between different regions. We have found that, while some peaks are indeed common, this is not true for all of them. The spectra in Figure 2b,c were fitted using a series of Gaussians. Figure 2b1-b6 and 2c1-c6 show the distribution of the amplitudes of these Gaussians when this decomposition was applied to the entire data-set. A few observations are in order. Firstly, by examining the energies of the peaks, we can see that peaks 1, 2 and 6 have similar central wavelengths, while the other 3 peaks are different. Secondly, there are strong differences in the way in which the peaks are distributed along the nanowire, with some showing strong maxima, while others appear relatively uniform.

Lastly, the decomposition allows us to visualize which areas are better fitted by spectra of the type shown in Figure 2b or 2c. This information is summarized in Figure 2d and Figure 2e, which are maps corresponding to the two spectra. The distribution appears to be somewhat random, with alternating preference towards each of the two components.

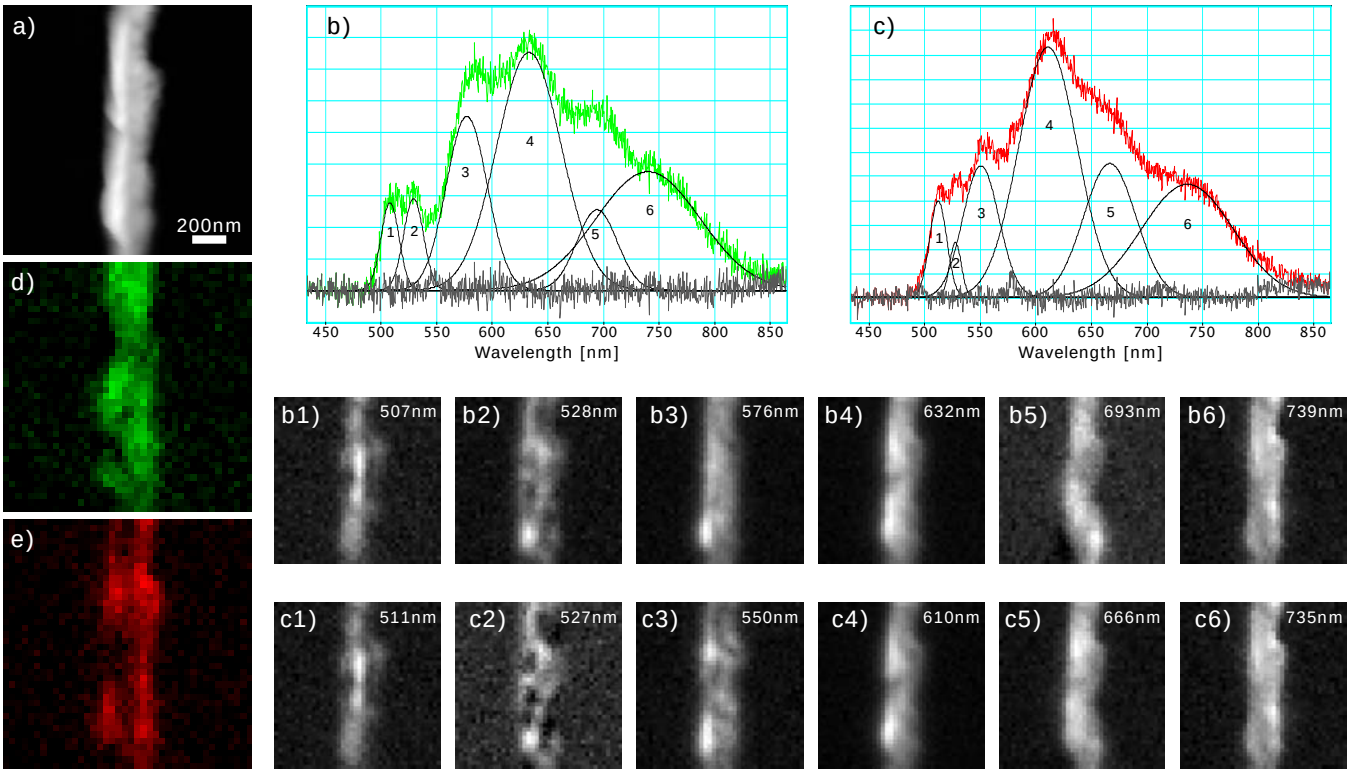

Figure 2. Cathodoluminescence mapping of a CdS nanowire. a) Annular dark-field image of the region of interest, corresponding to the end-section of a nanowire. b,c) Spectra obtained from two different parts of this region. The Gaussian components of each of the spectra are indicated using solid lines. Fitting residuals are indicated in gray. b1-b6, c1-c6) Spatial distribution of the amplitudes corresponding to the Gaussian components of the two spectra. d,e) Maps of the regions corresponding to spectra of type b) or c), respectively. The Gaussian decomposition of the data-set was performed by employing non-linear least-squares (NLLS) fitting.

Given the complicated nature of our findings, we have performed several control experiments in order to identify possible causes behind the behavior of the NWs. The results are summarized in Figure 3, which compares CL and photoluminescence (PL) data taken on similar NWs. Figure 3a shows a series of spectra obtained, in each case, by averaging over the signals obtained from the entire region of interest. The figure indicates that, while there are some common features found in many of the spectra, there is also significant variation between the data, despite the similar nature of the samples and experiments.

Figure 3b illustrates a series of PL data acquired on as-grown CdS NWs and a second series which was taken from NWs which had previously been irradiated inside the TEM, under comparable conditions to the ones subjected to CL mapping. The

data shows clear similarities between the structures within the same series, as well as between the irradiated and non-irradiated NWs.

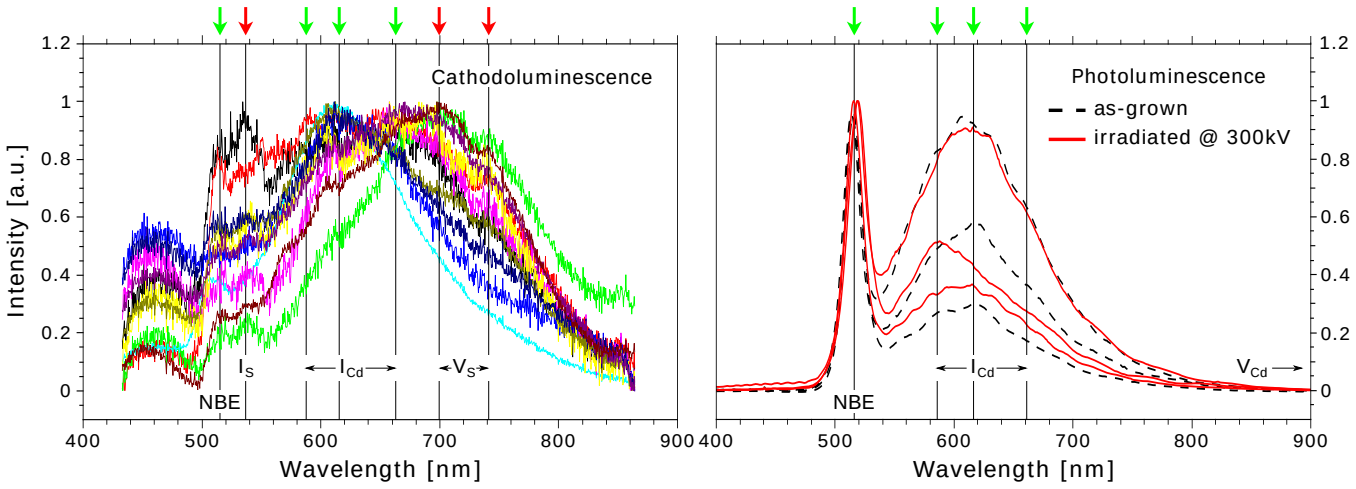

Figure 3. a) Spatially-averaged cathodoluminescence spectra for different nanowires. b) Photoluminescence spectra acquired from different as-grown (dashed lines) and electron-irradiated (full lines) nanowires. The spectra have been normalized for ease of comparison. Green arrows mark peaks which are common to the two panels, while newly-observed peaks are indicated using red arrows.

The principles behind CL experiments inside the TEM are described in Ref. 11. As the electrons pass through the material, some of them undergo inelastic scattering and lead to the production of electron-hole pairs. The recombination of these pairs is accompanied by the emission of photons. The recombination process is enhanced by the presence of defects in the material, creating energy levels within the band-gap which trap the carriers and act as recombination centers. The limiting factor which determines the resolution of the technique is the diffusion length of the generated carriers. Values as low as 2R=25 nm have been proposed by theoretical calculations reprinted in Ref. 11, but measured values on individual CdS NWs give larger values of around 100 nm.[12] Our measurements are in agreement with the latter value.

It is important to investigate the physical reasons behind the various peaks observed in our experiments. In the absence of doping and in view of the single-crystal nature of our samples, the primary candidate structures are atomic-scale intrinsic defects. Spectra, such as the ones obtained by PL in Figure 3b, contain two distinct regions: the sharp peak centered around 515 nm, associated with near-band emission (NBE), since the energy corresponding to this wavelength (2.4 eV) is close to reported values for the room-temperature band-gap of CdS,[13] and the wider peak centered around 600-650 nm, historically associated with defects.[14]

Despite the fact that research on the luminescence of CdS goes back to the 1950s, there is significant disagreement in the literature when it comes to assigning the various peaks to certain defects. This is partly due to the lack of direct evidence for these defects. In order to overcome this, several groups have performed luminescence measurements on CdS structures after exposing them to conditions which would favor different types of defects. This was done through electron irradiation at different voltages,[15,16] by annealing in Cd- or S-rich atmospheres[17-19] or through chemical treatments.[20] By analyzing and averaging over all of the findings, we can assign the green 520-530 nm band to S interstitials, orange 600-650 nm region to Cd interstitials, red 680-770 nm region to S vacancies, and finally, the near-infrared (NIR) 1000-1030 nm region to Cd vacancies.

By relating the above with PL data in Figure 3, we can conclude that the as-grown NWs contain primarily defects under the form of Cd interstitials. These peaks also appear in the CL data and are marked with green arrows. While our system does not allow us to perform NIR PL on individual structures, similar measurements performed on the NW powder, displayed in Figure S2 in the supplementary material, show a broad peak in the 1000-1100 nm region and also indicate the presence of Cd vacancies for the as-grown NWs. The differences which exist between the spectra in Figure 3a and 3b, marked by red arrows, imply that some of the defects responsible for luminescence in the former case are produced as a result of electron irradiation.

Electron irradiation damage is unavoidable, considering the high acceleration voltage and probe currents used during the experiments. Under the present conditions, damage in this material proceeds by atomic displacements as a result of elastic collisions with the high energy electrons.[21] The threshold energies (and corresponding electron acceleration voltages) for S and Cd in CdS have been measured to be 8.7 eV (115 keV)[15] and 7.3 eV (290 keV).[16] Based on these energy values, the displacement cross-sections calculated using a model from Ref. 22 are 5 times larger for S atoms (100 bn) than for Cd atoms (20 bn). This leads to displacement rates of ~1 displ s^{-1} for S atoms and ~0.2 displ s^{-1} for Cd. Considering the scanning speed of the electron beam, we estimate one S vacancy every 50x50 nm^2 and one Cd vacancy every 135x135 nm^2. These values lead to defect concentrations which are low and difficult to measure using traditional techniques, but which can act as luminescence centers.

Figure 3a shows that the electron beam creates defects corresponding to two regions: between 500 and 550 nm, in the green band – corresponding to S interstitials – and between 650 and 800 nm, in the red band – corresponding to S vacancies. According to Figure 2, the way in which these peaks are distributed is different: the first group features localized maxima, while the second group is distributed uniformly across the surface of the sample. This is to be expected since, according to

the calculations in the previous paragraph, the average distance between S vacancies is lower than the carrier diffusion length. Moreover, the 740 nm peak appears to have maxima close to the right-side edge of the NW, where the thickness is minimal. This is in agreement with our electron damage hypothesis, since there is a higher probability of damage occurring in thinner areas of the sample, where a larger percentage of the atoms are found close to the surface.

A final interesting point is the similarity between the PL spectra on as-grown and electron-irradiated NWs in Figure 3b. The optical absorption coefficient for the 325 nm excitation wavelength in CdS is $2 \cdot 10^5$ cm^{-1},[23] which gives a penetration depth of around 50 nm. Coupled with the 100 nm carrier diffusion length, this excludes the possibility that the defects are out of reach. Possible explanations are that the defects are unstable and that they recover during the time interval between the two experiments (typically a few hours), or that the laser used does not (preferentially) excite these centers.

To conclude, we have performed CL studies on CdS nanowires inside a TEM. We have observed that the electron beam used for analysis creates, in this particular case, new defects in the material, and we have exploited this fact in order to characterize them. We assign a ~740 nm luminescence peak to S vacancies and a 530 nm peak to S interstitials, which are a by-product of the same damage process. This is fully supported by our calculations concerning irradiation damage in this material and in agreement to previously reported data. Our technique allows us to map these signatures with nanometer precision, providing new insight into the nature and distribution of defects in CdS nanowires.

See supplementary material for images and diffraction data of a NW, as well as for NIR PL data acquired from the NW sample, as powder.

The authors would like to thank Dr. Martin Elborg (NIMS) for the NIR PL measurements and Dr. Yoshio Bando (NIMS) for valuable discussions. Funding was provided by the National Institute for Materials Science (NIMS) through the International Center for Materials Nanoarchitectonics (MANA). O.C. is grateful to the International Center for Young Scientists (ICYS) of NIMS for financial support.

References

[1]D. B. Williams, C. B. Carter, *Transmission Electron Microscopy: A Textbook for Materials Science*, Springer, 2009.

[2]F. Banhart, *In-Situ Electron Microscopy at High Resolution*, World Scientific, 2008.

[3]T. Xu, L. Sun, Small 2015, 27, 3247.

[4]B. G. Yacobi, D. B. Holt, *Cathodoluminescence Microscopy of Inorganic Solids*, Springer, 1990.

[5]N. Yamamoto, Mater. Trans., JIM 1990, 31, 659.

[6]T. Kizuka, M. Oyama, J. Nanosci. Nanotechnol. 2011, 11, 3278.

[7]Y. Xia, P. Yang, Y. Sun, Y. Wu, B. Mayers, B. Gates, Y. Yin, F. Kim, H. Yan, Adv. Mater. 2003, 15, 353.

[8]N. V. Hullavarad, S. S. Hullavarad, P. C. Karulkar, J. Nanosci. Nanotechnol. 2008, 8, 3272.

[9]C. Zhang, Z. Xu, W. Tian, D.-M. Tang, X. Wang, Y. Bando, N. Fukata, D. Golberg, Nanotechnology 2015, 26, 154001.

[10]W. S. Rasband, U. S. National Institutes of Health, Bethesda, Maryland, USA, http://imagej.nih.gov/ij/ (1997-2016).

[11]G. Dehm, J. M. Howe, J. Zweck, *In-situ Electron Microscopy: Applications in Physics, Chemistry and Materials Science*, John Wiley & Sons, 2012.

[12]Y. Gu, J. P. Romankiewicz, J. K. David, J. L. Lensch, L. J. Lauhon, E.-S. Kwak, T. W. Odom, J. Vac. Sci. Technol., B 2006, 24, 2172.

[13]O. Madelung, U. Rössler, M. Schulz, *Landolt-Börnstein - Group III Condensed Matter*, Vol. 41B, Springer, 1999.

[14]A. A. Vuylsteke, Y. T. Sihvonen, Phys. Rev. 1959, 113, 1.

[15]B. A. Kulp, R. H. Kelley, J. Appl. Phys. 1960, 31, 1057.

[16]B. A. Kulp, Phys. Rev. 1962, 125, 1865.

[17]O. Vigil, I. Riech, M. Garcia-Rocha, O. Zelaya-Angel, J. Vac. Sci. Technol., A 1997, 15, 2282.

[18]N. Susa, H. Watanabe, M. Wada, Jpn. J. Appl. Phys. 1976, 15, 2365.

[19]N. A. Vlasenko, N. I. Vitrikhovskii, Z. L. Denisova, V. F. Pavlenko, Opt. Spectrosc. 1966, 21, 261.

[20]J. J. Ramsden, M. Grätzel, J. Chem. Soc., Faraday Trans. 1 1984, 80, 919.

[21]F. Banhart, Rep. Prog. Phys. 1999, 62, 1181.

[22]J. C. Meyer, F. Eder, S. Kurasch, V. Skakalova, J. Kotakoski, H. J. Park, S. Roth, A. Chuvilin, S. Eyhusen, G. Benner, A. V. Krasheninnikov, U. Kaiser, Phys. Rev. Lett. 2012, 108, 196102.

[23]C. Honsberg, S. Bowden, PVCDROM, http://www.pveducation.org/pvcdrom/absorption-coefficient .